Slip flow over structured surfaces with entrapped microbubbles

Jari Hyväluoma[1] and Jens Harting[2]

[1] *Department of Physics, University of Jyväskylä, FI-40014 Jyväskylä, Finland*
[2] *Institute for Computational Physics, Pfaffenwaldring 27, D-70569 Stuttgart, Germany*
(Dated: May 26, 2008)

On hydrophobic surfaces, roughness may lead to a transition to a superhydrophobic state, where gas bubbles at the surface can have a strong impact on a detected slip. We present two-phase lattice Boltzmann simulations of a Couette flow over structured surfaces with attached gas bubbles. Even though the bubbles add slippery surfaces to the channel, they can cause negative slip to appear due to the increased roughness. The simulation method used allows the bubbles to deform due to viscous stresses. We find a decrease of the detected slip with increasing shear rate which is in contrast to some recent experimental results implicating that bubble deformation cannot account for these experiments. Possible applications of bubble surfaces in microfluidic devices are discussed.

PACS numbers: 83.50.Rp, 47.55.D-, 47.11.-j

The no-slip boundary condition states that the fluid velocity at a fluid-solid interface equals to that of the solid surface. Although this boundary condition has been proven valid at macroscopic scales, it has no microscopic justification and is not fulfilled generally [1]. Its validity was debated already in the early days of fluid mechanics and due to recent developments in microfluidics the interest in violation of the no-slip boundary condition has revived [2]. In microfluidics, several experiments have found fluid slip at the boundaries of the flow channels [3, 4]. As the slip length (defined below) has typically a magnitude measured in nano- or micrometers, the appearance of slip does not have noticeable ramifications in macroscopic flows. However, in microfluidic devices with large surface-to-volume ratio, surface properties may dramatically affect the flow resistance. The possibility to engineer slip properties in a controlled way is therefore crucial for microfluidic applications.

The slip at fluid-solid boundaries can be quantified by Navier's boundary condition, which states that the slip velocity is proportional to the velocity gradient, i.e., $v_s = b(\partial v/\partial z)$ at the surface $z = z_0$. Here, b is the slip length which is the distance below the surface where the velocity linearly extrapolates to zero. Higher slip length means larger slip and lower friction at the boundary.

Mechanisms behind boundary slip include surface roughness and structural characteristics of roughness [5, 6], roughness-induced dewetting on hydrophobic surfaces [7, 8], dissolved gas and bubbles on the surface [9, 10, 11], as well as wetting properties [12]. Usually, roughness decreases the slip length due to increased dissipation and the roughness induced slip is just an artifact [5]. Theoretically, it was shown that even slippery surfaces, if rough enough, can provide no-slip boundaries [13]. However, if surfaces are hydrophobic, roughness may increase the slip due to a transition to a superhydrophobic (fakir or Cassie) state [14]. Here, liquid cannot enter between roughness elements but stays at the top of them. Thus, gas bubbles or layers are formed

thereby lubricating the flow due to a reduced liquid-solid contact area. By using a surface patterned with a square array of cylindrical holes, Steinberger et al. found that gas bubbles may also cause an opposite effect, i.e., slip is reduced if microbubbles are present in the holes [10]. Numerically, they found even negative slip lengths for flow over such a bubble mattress. Negative slip means that the effective no-slip plane is inside the channel, i.e., the bubbles increase the flow resistance. These mechanisms are related to so-called effective slip and should be distinguished from the (smaller) intrinsic slip on smooth surfaces. Another peculiarity in the boundary slip is the shear-rate dependence observed in some experiments but not in the others [2]. The question if the shear-rate dependence is a true property of slip is still to be answered.

As the different mechanisms behind the slip phenomenon are strongly intertwined, the experimental study of a single mechanism is a complicated task. Therefore, numerical simulations are attractive as they provide a controllable way to change a single property of fluid or surface while keeping the others unchanged. Most computer simulations so far have been performed using molecular dynamics [7, 15, 16, 17]. For computational reasons molecular dynamics is limited to length scales of tens of nanometers and time scales of nanoseconds, which do not comply with the experimentally relevant scales. Therefore, mesoscopic lattice Boltzmann (LB) simulations have recently been applied to study flow in microchannels or along hydrophobic surfaces [5, 8, 12, 18, 19]. This method allows to reach experimentally relevant scales and preserves those interactions needed to describe the underlying physics.

Our simulations utilize the multiphase LB model by Shan and Chen [20]. Dynamics of the method is governed by a discretized Boltzmann equation

$$f_i(\mathbf{r} + \mathbf{c}_i, t+1) - f_i(\mathbf{r}, t) = -\frac{1}{\tau}\left[f_i(\mathbf{r}, t) - f_i^{eq}(\mathbf{r}, t)\right], \quad (1)$$

where f_i is a distribution function describing the probability to find a particle at position $\mathbf{r}$ at time step t, mov-
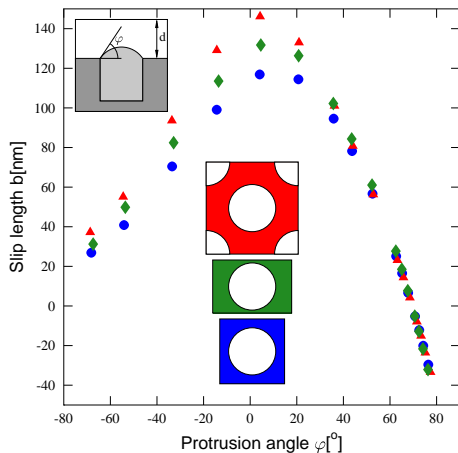
FIG. 1: (Color online) Slip length b as a function of protrusion angle φ. A unit cell of each array is shown in insets and corresponding results are given by triangles (rhombic array), diamonds (rectangular array), and circles (square array). The inset in the top-left corner shows the definition of φ.

ing in lattice direction $\mathbf{c}_i$. We use a three-dimensional lattice with 19 discrete velocities. The right-hand side of Eq. 1 models the relaxation of the f_i towards a local equilibrium due to collisions among the particles on a time scale given by the relaxation time τ. The mean-field interactions between particles are given by a force

$$\mathbf{F} = G_b \psi(\mathbf{r}) \sum_i t_i \psi(\mathbf{r} + \mathbf{c}_i) \mathbf{c}_i, \qquad (2)$$

where $\psi = 1 - \exp\left(-\rho/\rho_0\right)$ is an effective mass (ρ is the fluid density, ρ_0 a reference density), G_b tunes the strength of the interaction, and t_i's are weight factors for different lattice directions. This force term leads to a non-ideal equation of state with pressure $P = c_s^2 \rho + \frac{1}{2} c_s^2 G_b \psi^2$, where c_s is the speed of sound, and it enables simulations of liquid-vapor systems with surface tension. To model the wetting behavior at fluid-solid surfaces, a similar interaction is added between the fluid and solid phases, and the contact angle is tuned by setting a density value ρ_w at the boundaries [21].

In this article we investigate liquid slip in Couette flow, where the flow is confined between two parallel walls. One of the walls is patterned with holes and vapor bubbles are trapped to these holes. Steinberger et al. [10] presented finite-element simulations of flow over rigid "bubbles" by applying slip boundaries at static bubble surfaces. The LB method allows the bubbles to deform if the viscous forces are high enough compared to the surface tension. We are also interested in how surface patterning affects the slip properties of these surfaces, and how bubbles could be utilized to develop surfaces with special properties for microfluidic applications.

In our simulations, the lower wall is static and has the topographical patterning whereas the upper one is

smooth and moved with velocity u_0. The distance between walls is $d = 1 \ \mu\text{m}$ (40 nodes) in all simulations, and the area fraction of holes 0.43 unless stated otherwise. The system boundaries are periodic and a unit cell of the regular array is included in a simulation. To trap bubbles to holes, some heterogeneity is needed at the edges of holes in order to pin the contact line. To this end, we use different wettabilities for boundaries in contact with the main channel and with the hole. The protrusion angle φ (see Fig. 1 for definition) is varied by changing the bulk pressure of the liquid. A similar technique to form bubbles on structured surfaces was used experimentally by Bremond et al. [22]. The effective slip length can be calculated from the shear stress $\sigma = \mu \text{d}v/\text{d}z$ acting on the upper wall, which is obtained from the no-slip boundary condition imposed at the fluid-solid boundaries. Thus the effective slip length reads as $b = \mu u_0/\sigma - d$, where μ is the dynamic viscosity of the liquid. b is measured from the top of the structured surface and G_b is chosen such that the density ratio between liquid and gas is 22. This ratio is too small for a realistic description of gas bubbles in a liquid. Also, the interface between both phases is of finite width causing the resistance in the vapor phase. These limitations of multiphase LB models do not influence the qualitative insight obtained from our simulations.

In order to study the effect of a modified protrusion angle and different surface patterns, we use three different arrays of bubbles, i.e., a square array, a rectangular array where the distance of bubbles is larger in one direction than in the other, and a rhombic array. These surfaces have cylindrical holes with radius $a = 500$ nm and the area fraction of the holes is equal in all cases. The shear rate is such that the Capillary number $Ca = 0.16$. The Capillary number is the ratio of viscous and surface forces, i.e., $Ca = \mu a G_s/\gamma$, where G_s and γ are the shear rate and surface tension, respectively. Snapshots of simulations are shown in Fig. 2 and the slip lengths obtained are shown in Fig. 1. The observed behavior is similar to that reported in [10], where a square array of holes was studied. In particular, we observe that when the protrusion angle is large enough the slip length becomes negative. We also see that the maximum of the slip length is obtained when the protrusion angle equals zero. Since the area fraction of the bubbles is the same in all three cases, the results clearly indicate that slip properties of the surface can be tailored not only by changing the protrusion angle but also by the array geometry.

Next, the shear-rate dependence of the slip length is investigated. As the shear rate and thus the viscous stresses grow the bubbles are deformed (see Fig. 2) and the flow field is modified. Results are shown in Fig. 3a, where the slip length is given as a function of the Capillary number for three different protrusion angles. We also calculate the Taylor deformation $D = (\ell - a)/(\ell + a)$ of the bubbles by fitting an ellipse to the bubble interface. Here, a and ℓ are the minor and major axes of
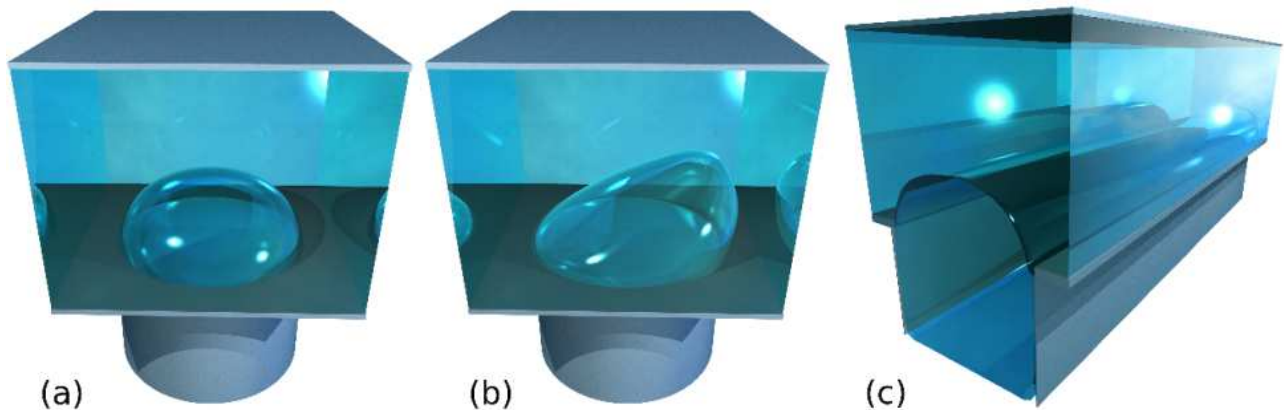
FIG. 2: (Color online) Snapshots of simulations of bubbles on structured surfaces. Shown are a square array of bubbles with Capillary number (a) $Ca = 0.02$ and (b) $Ca = 0.4$, and (c) a slot with a cylindrical bubble. In each case a unit cell is shown.
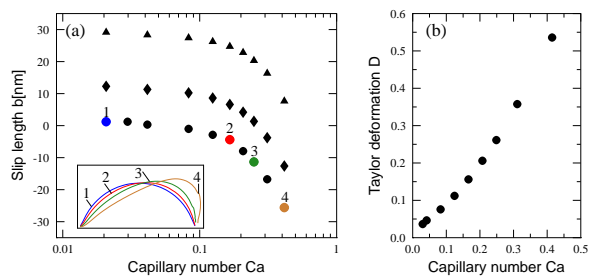

FIG. 3: (Color online) (a) Slip length as a function of capillary number for a square array of bubbles with three different protrusion angles, $\varphi = 63°, 68°$, and $71°$ (from uppermost to lowermost). In the inset shown are cross sections of liquid-gas interfaces for four capillary numbers. (b) Taylor deformation as a function of Capillary number for the bubble with $\varphi = 71°$. These Ca values correspond to shear rates of the order of $10^{-6} - 10^{-7} \text{ s}^{-1}$.
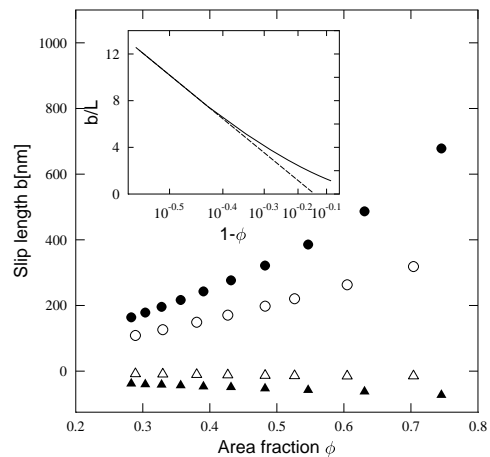

FIG. 4: Slip length as a function of hole area fraction. Filled circles denote values for the flow parallel to the slots and triangles relate to the perpendicular direction. Corresponding open symbols are for a surface with rectangular holes ($\varphi = 72°$). The inset shows the normalized slip length as a function of the solid-area fraction, where the dashed line is the theoretical prediction for small solid-area fractions.

the ellipse, respectively. A slightly superlinear relation between D and Ca is observed (Fig. 3b) in accordance with a two-dimensional case in Ref. [23]. We find that increasing shear rates cause the slip length to decrease. This behavior is contradictory to those found in some experiments using surface force apparatuses (see, e.g., Ref. [24]), where a strong increase in the slip is observed after some critical shear rate. This shear-rate dependence has been explained, e.g., with formation and growth of bubbles [9, 11]. However, one should notice that these experiments are dynamic in nature while we simulate a steady case. In our simulations there is no formation or growth of the bubbles but we determine the slip for given bubbles of given size. Our results indicate that the deformation of the bubbles and the changes in the flow field thereby occurring cannot be an explanation for the observed shear-rate dependence. On the other hand, our results are consistent with [5], where it is shown that smaller roughness leads to smaller values of a detected slip. In the present case, the shear reduces the average

height of the bubbles and thus the average scale of the roughness decreases as well.

As seen above, the slip properties of a bubble mattress can be tailored by changing the surface patterning. Next, we consider a surface which has slots with a width of $1 \mu\text{m}$, and cylindrical bubbles protruding to the channel with an angle $\varphi = 72°$ (Fig. 2c). We apply shear parallel and perpendicular to the slots, while the area fraction of the bubbles (ϕ) is varied by changing the distance between the grooves (L). According to our results (Fig. 4), b strongly depends on the flow direction and even the qualitative behavior changes. When the flow is parallel to the slot a positive slip is observed, but for perpendicular flow the slip becomes negative. This observation

can be explained by means of theoretical predictions of Richardson, who showed that slippery surfaces lead to (macroscopic) no-slip boundaries if rough enough [13]. Our results support these predictions. In the case with flow parallel to the bubbles the streamlines are straight and the flow does not "see" any roughness. However, in the perpendicular direction roughness is caused by the bubbles and negative slip is observed. The inset of Fig. 4 depicts the scaling behavior of the slip length as a function of the solid-area fraction for flow perpendicular to the slots. We see that for small solid-area fraction the slip length obeys the scaling law $b \sim -L \log(1 - \phi)$ as was recently predicted in Ref. [6]. Anisotropic behavior has been observed in the case of flat surfaces composed of stripes with no-slip and perfect-slip boundary conditions [25, 26]. Our simulations differ from these studies as our bubbles protrude to the channel thus leading to a larger effect than for a flat surface. In order to understand less idealized surface patternings, we study flow over rectangular holes. The aspect ratio of the holes is chosen such that the longer side is three times the smaller one. We observe similar qualitative behavior (Fig. 4), but the difference in slip length between the two flow directions is less pronounced. Obviously, by changing the aspect ratio of the hole, the anisotropic behavior of the slip can be tailored. Due to the striking difference between the slip properties in the two perpendicular directions, we believe that this kind of surfaces may find applications in microfluidic devices. Anisotropic surfaces could be used to suppress the flow in an unwanted direction while enhancing it in another one. The suppressing behavior is further amplified by the shear-rate dependence, since the negative slip is growing with the shear rate.

To conclude, we simulated Couette flow in a microchannel where one of the walls is patterned and microbubbles are attached to the pattern. We found that the slip properties of the surface can be tailored by changing the hole array and that such a surface with bubbles may yield negative slip, i.e., increased resistance to flow, if bubbles are strongly protruding to the channel. Our results can be qualitatively compared to previous results [10], but overcome their limitation of a static liquid-vapor interface. This allowed to study the influence of the shear rate on the deformation of the interface and it's effect on the measured slip. We found that the slip decreases with increasing shear rate demonstrating that shear induced bubble deformation cannot explain recent experimental findings where slip increases with increasing shear rate [24]. We proposed a special surface patterning which can be used to produce surfaces where the slip is positive in one direction and negative in the perpendicular one. Such a surface might be useful to construct microfluidic devices with tunable flow throughput which could be controlled by adding bubble ridges parallel or perpendicular to the flow. In addition, we have shown that the throughput could be tailored by tuning the bulk pressure, i.e., the protrusion angle, or the shear rate.

[1] E. Lauga, M. Brenner, and H. Stone, in *Handbook of Experimental Fluid Mechanics*, edited by C. Tropea, A.L. Yarin, and J.F. Foss (Springer-Verlag, Berlin, 2007).
[2] C. Neto, D.R. Evans, E. Bonaccurso, H.-J. Butt, and V.S.J. Craig, Rep. Prog. Phys. **68**, 2859 (2005).
[3] D.C. Tretheway and C.D. Meinhart, Phys. Fluids **14**, L9 (2002).
[4] P. Joseph, C. Cottin-Bizonne, J.-M. Benoît, C. Ybert, C. Journet, P. Tabeling, and L. Bocquet, Phys. Rev. Lett. **97**, 156104 (2006).
[5] C. Kunert and J. Harting, Phys. Rev. Lett. **99**, 176001 (2007).
[6] C. Ybert, C. Barentin, C. Cottin-Bizonne, P. Joseph, and L. Bocquet, Phys. Fluids **19**, 123601 (2007).
[7] C. Cottin-Bizonne, J.-L. Barrat, L. Bocquet, and E. Charlaix, Nature Mater. **2**, 237 (2003).
[8] M. Sbragaglia, R. Benzi, L. Biferale, S. Succi, and F. Toschi, Phys. Rev. Lett. **97**, 204503 (2006).
[9] P.G. de Gennes, Langmuir **18**, 3413 (2002).
[10] A. Steinberger, C. Cottin-Bizonne, P. Kleimann, and E. Charlaix, Nature Mater. **6**, 665 (2007).
[11] E. Lauga and M.P. Brenner, Phys. Rev. E **70**, 026311 (2004).
[12] J. Harting, C. Kunert, and H.J. Herrmann, Europhys. Lett. **75**, 328 (2006).
[13] S. Richardson, J. Fluid Mech **59**, 707 (1973).
[14] A. Lafuma and D. Quéré, Nature Mater. **2**, 457 (2003).
[15] J. Koplik and J.R. Banavar, Annu. Rev. Fluid Mech. **27**, 257 (1995).
[16] P.A. Thompson and S.M. Troian, Nature **389**, 360 (1997).
[17] J.-L. Barrat and L. Bocquet, Phys. Rev. Lett. **82**, 4671 (1999).
[18] R. Benzi, L. Biferale, M. Sbragaglia, S. Succi, and F. Toschi, Europhys. Lett. **74**, 651 (2006).
[19] J. Hyväluoma, A. Koponen, P. Raiskinmäki, and J. Timonen, Eur. Phys. J. E **23**, 289 (2007).
[20] X. Shan and H. Chen, Phys. Rev. E **47**, 1815 (1993); **49**, 2941 (1994).
[21] R. Benzi, L. Biferale, M. Sbragaglia, S. Succi, and F. Toschi, Phys. Rev. E **74**, 021509 (2006).
[22] N. Bremond, M. Arora, C.-D. Ohl, and D. Lohse, Phys. Rev. Lett. **96**, 224501 (2006).
[23] J.Q. Feng and O.A. Basaran, J. Fluid Mech. **275**, 351 (1994).
[24] Y. Zhu and S. Granick, Phys. Rev. Lett. **87**, 096105 (2001).
[25] J.R. Philip, Z. Angew. Math. Phys. **23**, 960 (1972).
[26] E. Lauga and H.A. Stone, J. Fluid Mech. **489**, 55 (2003).